CHEMISTRY OF MATERIALS

ARTICLE

pubs.acs.org/cm

Preparation and Characterization of Monodisperse Fe_3O_4 Nanoparticles: An Electron Magnetic Resonance Study

Javier Salado,[†] Maite Insausti,[†] Luis Lezama,[†] Izaskun Gil de Muro,[†] Eider Goikolea,[‡] and Teófilo Rojo*[,†,‡]

[†]Inorganic Chemistry, Zientzia eta Teknologia Fakultatea, UPV/EHU, Sarriena auzoa, 48940 Leioa, Spain

[‡]CICenergiGUNE, Parque Tecnológico, Albert Einstein, 48, 01510 Miñano, Spain

Supporting Information

ABSTRACT: One of the major challenges prior to a proper application of magnetic iron oxide nanocrystals is not only to understand the influence of the synthetic parameters on the final characteristics of the nanoparticles but also to optimize characterization methods in order to understand the magnetic behavior. First, a systematic study of the different parameters on a facile chemical synthetic route based on the thermal decomposition of iron(III) acetylacetonate, allowed a fine adjustment of the synthetic conditions to obtain oleic acid and oleylamine capped magnetite nanoparticles with perfectly defined size within 3.5−7 nm in diameter and organic content from 16.1 to 40.9%. Second, a complete characterization of samples by means of electron magnetic resonance (EMR) as a function of the angle and temperature was carried out. This technique allows to accurately elucidate the key characteristics of the deviation from the ideal superparamagnetic behavior observed in some samples by magnetic measurements. The optimization of the sample-handling for the EMR measurements emerged as a decisive step to provide reproducible results and to ultimately demonstrate that the lack of organic content adsorbed on the nanoparticle surface favored a ferromagnetic behavior. Furthermore, resonance lines ascribed to forbidden $\Delta M_S = \pm 2$ transitions were observed in the EMR spectra of this system, which open up new research possibilities for evaluating interparticle interactions.

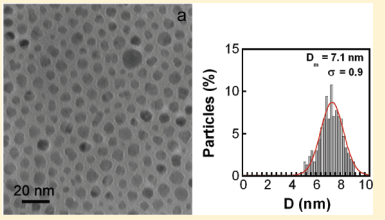

KEYWORDS: Nanoparticles, nanomaterials, magnetism, electron magnetic resonance

1. INTRODUCTION

Because of the current interest in implementing nanostructured materials in different technological areas, as well as from the fundamental scientific point of view, it is of great relevance the precise knowledge on the characteristics that rule their novel properties.[1] To study the properties of a material, it is critical to fabricate monodisperse nanoparticles with a perfectly controlled size owing to the strong size-dependence of properties.[2−4] Sample uniformity in terms of size, morphology, internal structure, and surface chemistry makes possible to distinguish the properties inherent to the material from those associated to structural heterogeneity and/or size and shape dispersion. Among the large variety of size-dependent physical properties, magnetic effects are of key importance since they show great attractive for a broad range of biomedical applications that, ultimately, could have a far reaching impact both in cancer diagnosis and therapy.[5] Within this scope, magnetite (Fe_3O_4) has become an important kind of magnetic material, emerging as a promising candidate for drug delivery,[6,7] hyperthermia,[8] or contrast enhancement in magnetic resonance imaging (MRI).[9] The main aspects that have given a boost to the study of magnetite nanoparticles are mainly their active surface chemical functionality, biocompatibility and low cost. Chemical stability is generally referred as another advantage however, under an aerobic atmosphere magnetite is often oxidized to maghemite (γ-Fe_2O_3) at the surface.

Thus, for these studies, apart from accurately controlling the size and particularly the size distribution, the synthesis method must also provide a way to avoid particle aggregation and protect the surface from oxidation. Recently, various wet chemical approaches using surfactants have been developed.[10] The reversible adsorption of organic ligands onto the surface during the synthesis mediates the growth, passivates the surface against oxidation and prevents particles from aggregation due to steric or electrostatic repulsion. Among these, the decomposition of organometallic precursors in organic solvents at high temperatures provides an efficient route to obtain highly crystalline and monodisperse particles with excellent magnetic properties.[11] In particular, the so-called polyol method has demonstrated to be an effective and reproducible route to prepare oleic acid and oleylamine capped magnetite nanoparticles,[12] in which sample characteristics can be fine-tuned by simply modulating synthetic parameters such as reaction time, temperature, solvent and the reagent and/or solvent concentration.[13]

Out of the most remarkable size dependent magnetic phenomena observed in fine particle systems, the most studied is the superparamagnetism,[14] typically observed when the size of a particle drops below a certain diameter and becomes comparable to the size of a magnetic domain.[15] In this regime, surface effects that occur because of defects, lack of symmetry, or uncoordinated atoms become more pronounced and they go into competition with finite size effects.[16] Consequently, the magnetization profile

Received: January 25, 2011
Revised: April 11, 2011
Published: May 20, 2011

across the particle is no longer uniform; the magnetization of the surface layer can indeed differ from the corresponding to the core spins. A secondary surface effect that can also uniquely affect magnetic properties is the additional electronic redistribution that emerges due to the capping.[17] Besides, the system under study is generally considered to be composed of non interacting particles so the physical properties depend solely on their inner characteristics, but in real systems, particles tend to agglomerate or are forced together through self-assembly, exhibiting a collective behavior as a result of magnetic coupling.[18]

The electron magnetic resonance (EMR) is a powerful and sensitive technique for the investigation of magnetic properties and magnetization dynamics of nanoparticles.[19] In this sense, while in dc magnetometry it is sometimes difficult to discriminate different magnetic contributions, those can be clearly distinguished by EMR, emerging the latter as an ideal tool to study system features that might be overlooked by dc magnetization measurements.

Herein, we present a detailed characterization by means of magnetic and EMR measurements of magnetite nanoparticles prepared via the polyol method. Within this aim and in order to establish a relationship between the magnetic behavior of samples and sample characteristics, a great effort has been devoted not only to obtain nanoparticles with different size and organic content but also to optimize EMR measuremets which could help to elucidate the different contributions observed in magnetic measurements with contradictory interpretations in the literature. The characterization has been completed by transmission electron microscopy (TEM) and thermogravimetric analysis.

2. EXPERIMENTAL SECTION

Materials. Iron(III) acetylacetonate (99.9%), 1, 2-hexadecanodiol (90%), oleic acid (98%), oleylamine (70%), phenyl ether (99%), benzyl ether (99%), and n-hexane (99%) were purchased from Sigma-Aldrich and used as received without further purification. Acetone was purchased from Panreac S.A.

Synthesis of Magnetite Nanoparticles. Monodisperse Fe_3O_4 nanoparticles were prepared by reducing an iron solution with a polyol. Briefly, concentrations of iron(III) acetylacetonate varying from 0.5 to 2 mmol were suspended in 20 mL of phenyl ether, or benzyl ether, together with 10 mmol of 1,2-hexadecanediol and concentrations of oleylamine and oleic acid varying from 3 to 9 mmol. The mixture was first heated at 200 °C under continuous stirring for 30 min and then brought to reflux for 2 h in an argon atmosphere. Upon heating, the reaction mixture turned dark brown, indicating the formation of Fe_3O_4 nanoparticles. After the solution was cooled to room temperature, the resulting nanoparticles were precipitated by adding acetone, causing the flocculation of the particles. The formed nanoparticles were separated from the supernatant by centrifugation and the solid was redispersed in hexane and this solution was again centrifuged to get rid of non ligand-capped particles and large aggregates. Nanoparticles were repeatedly precipitated, adding acetone to the hexane solution and the final product was last isolated by filtering off the solution. A systematic study of the different synthetic parameters allowed us to obtain a series of samples showing different features. Out of all the prepared samples, five representative samples have been chosen and these will be designated throughout this paper as MNPX, where X refers to the approximate organic content.

Preparation of Nanoparticle Arrays and Monolayer Films. With the aim of avoiding the aggregation of the nanoparticles and getting dispersions where the interparticle interactions were minimized, the sample preparation was optimized to develop reproducible measurements in EMR. In this sense two different approaches were carried out. In the former, dispersed nanoparticles were deposited on a 2 × 10 mm dimension piece of filter paper. For this task, the paper was dipped into a dispersion of Fe_3O_4 nanoparticle in hexane and then lifted out of the colloidal suspension vertically. We fabricated the Fe_3O_4 nanoparticle array samples using different concentration of the Fe_3O_4 nanoparticles in solution.

In the second approach, magnetite nanoparticle monoloyer films were prepared by gently spreading 50 μL of a colloidal suspension of the hydrophobic nanoparticles in hexane on a Petri dish containing water. Upon solvent evaporation, the nanoparticles self-assemble into monolayer rafts floating on the surface of water. The resultant nanoparticle monolayer film formed at the air water interface was transferred to an acetate substrate by immersing it into the aqueous phase at an angle of 5−10° and the monolayer was deposited onto the substrate simply by pulling it slowly from the solution.

The Fe_3O_4 nanoparticle monolayer films were also transferred onto carbon-coated Cu grids and characterized by transmission electron microscopy to confirm the formation of a homogeneous film (see the Supporting Information).

Characterization. Microanalyses were performed with a Perkin-Elmer 2400 CHN analyzer. Thermogravimetric measurements were performed in a Netzsch STA 449 C thermogravimetric analyzer. Crucibles containing 7 mg of sample were heated at 10 °C min^{-1} under dry argon or air atmosphere. TEM micrographs were obtained using a Philips CM200 microscope at an acceleration voltage of 200 kV. For preparing the samples, powders were dispersed in hexane and dropped-cast onto copper grid. The magnetite nanoparticle monolayer films were also transferred onto Cu grids in order to be characterized by TEM. Magnetic measurements of powdered samples were carried out in the temperature range 1.8−300 K using a Quantum Design MPMS-7 SQUID magnetometer at magnetic fields between 0 and 7 T. EMR spectra were recorded on a Bruker ELESYS spectrometer, equipped with a standard Oxford low-temperature device operating at X band. For the angular measurements the sample films were immobilized on an L-shaped rack and mounted on a rotating support, and the EMR spectra for different sample orientations were obtained with an accuracy of ±0.1°.

3. RESULTS AND DISCUSSION

X-ray diffractograms of the samples can be indexed to face centered cubic phase of Fe_3O_4 (S.G.: $Fd3\overline{m}$, JCPDS No. 89−0691). From the broad maxima commonly observed in the diffraction patterns of nanophase materials it is difficult to completely discard the presence of maghemite, as it possesses a similar structure to magnetite with comparable cell parameters heading to nearly identical X-ray diffraction pattern.[20] Nevertheless, the low-angle region profile indicates magnetite as the principal phase.

All TEM micrographs of the synthesized samples show spherical particles and isolated one from another forming an assembly (Figure 1). To determine the average diameter and the size distribution, we fitted the size histogram data to a Gaussian function and values ranging from 3.5 ± 0.5 to 7.1 ± 0.9 nm were obtained depending on the employed synthesis conditions, as summarized in Table 1. Not only the concentration of reagents, but also the solvent and the stirring method were changed to correlate them with the dispersion and size of the magnetic nanoparticles obtained. One of the main factors influencing the final particle size is the stirring method. Indeed, when magnetic stirring was employed the particle size increased by 1 nm compared to the size obtained by mechanical stirring, as magnetic nuclei would aggregate around the magnetic stirring bar leading to increased sizes. Furthermore, the iron precursor concentration was directly related with particle size when magnetic stirring was used,

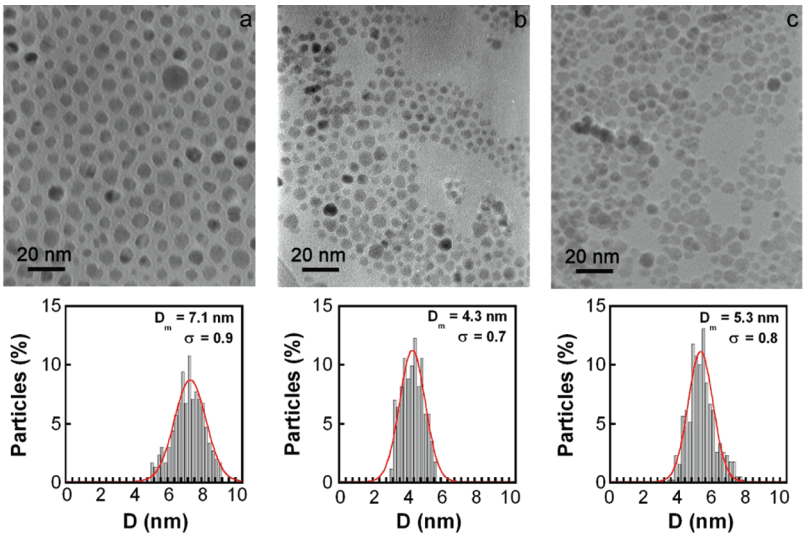

Figure 1. Transmission electron micrographs of (a) MNP18, (b) MNP30, and (c) MNP40 along with their corresponding histograms, where the solid line represents the fitting curve assuming a Gaussian function. The calculated mean particle diameter (D_m) and the standard deviation (σ) are shown in the histograms.

such as particle size slightly increased with increasing iron precursor concentration. Nevertheless, the use of mechanical stirring in the synthesis seems to assist the adsorption of the ligands onto the surface, avoiding particle growth. In this case, variations either in iron precursor or in oleylamine and oleic acid concentrations do not seem to play an important role in final particle size. Syntheses carried out using mechanical stirring method and keeping the concentration of both oleic acid and oleylamine constant to 6 mmol yielded the formation of the smallest nanocrystals of 3.5−4.5 nm regardless of the iron concentration. In these conditions, samples with the lowest standard deviation value in diameter have been obtained, forming hexagonal 2D self-assemblies in the Cu grid upon evaporation of the solvent.[21] Replacing the solvent from phenyl ether to benzyl ether under the conditions outlined above yielded slightly larger nanoparticles of 6 nm but with a higher dispersion in size, which appears to be undesirable for our subsequent magnetic studies.

Thermogravimetric analysis (TGA) curves of the magnetite powders show a well-defined mass loss profile over a temperature range of 200−450 °C (see the Supporting Information), attributed to decomposition of the organic ligands attached to the particle surface, which are mainly oleic acid molecules as was confirmed by microanalysis and infrared spectra. In fact, the $-COO^-$ group has higher affinity than the $-NH^-$ group of the deprotonated oleylamine to the iron oxide surface, although the presence of both ligands is necessary to maintain a kinetic control of growing conditions. Besides, the observed weight loss associated to the organic content differs remarkably among studied samples, ranging from 16.1 to 40.9% (Table 1). The higher organic content corresponds to samples with smallest particle size, which accounts for the larger total surface area in the sample.

Nevertheless, it has been observed that reagent concentrations also affect the organic content, particularly the molar ratio of oleic acid to oleylamine. In this sense, when this ratio was increased above 1, the reproducibility of the method was lost and remarkable differences in the organic content were observed in samples prepared using similar conditions. For example, a molar ratio of oleic acid to oleylamine of 2 yields organic contents of 39.6 and 54.6% for nanoparticles of 4.1 ± 0.7 and 3.8 ± 0.4 nm, respectively, indicating the importance of oleylamine in the synthesis procedure. Consequently, in order to obtain nanoparticles of similar size and organic content, molar ratios smaller than 1 are required.

The inorganic residue at the end of the thermal treatment was characterized by X-ray diffraction and the obtained diffraction pattern differed depending on the employed atmosphere. In the case of an air atmosphere, observed maxima were assigned to α-Fe_2O_3 (S.G.: $R3\bar{c}$, JCPDS No. 79−1741). On the contrary, when sample was heated under Ar atmosphere, in addition to the Fe_3O_4 phase, the residue also consisted of metallic iron (S.G.: $Im3\overline{m}$, JCPDS No. 06−0696) and $Fe_{0.925}O$ (S.G.: $Fd3\overline{m}$, JCPDS No. 89−0691), confirming the partial reduction of Fe_3O_4.

The magnetization curves of the samples were taken in zero-field-cooling (ZFC) and field-cooling (FC) modes under an applied magnetic field of 100 Oe (Figure 2). Magnetization values were converted into emu/g_{Fe3O4} units by calculating the magnetite mass from thermogravimetry results. In all cases the ZFC curve reaches a maximum at a blocking temperature (T_B) and, usually, just below this temperature the two curves split. However, there are also some differences that suggest two different magnetic behaviors among samples. On the one hand, in samples like MNP41 the transition to a blocked state occurs at a temperature $T_B < 40$ K and the magnetization relaxes sharply back to zero at room temperature, a feature that is consistent with a superparamagnetic behavior. On the other hand, samples as MNP16 show a broad magnetization maximum at $T_B \approx 80$ K and the magnetization decreases smoothly with increasing temperature, suggesting a ferromagnetic-like behavior owing to possible interparticle interactions. This shifting of the T_B and change in the magnetization evolution with temperature has been previously reported and was related to the different size that presented the nanoparticles.[22] However, as occurs with samples MNP30 and MNP41, magnetite samples from the present study show very different curve profiles despite their similar size. Therefore, additional facts should be taken into account to explain this behavior, as suggested by Mørup et al. in earlier studies involving samples of magnetic nanoparticles.[23]

dx.doi.org/10.1021/cm200253k |*Chem. Mater.* 2011, 23, 2879–2885

Table 1. Particle Radii Determined by TEM, Organic Content Determined by Thermogravimetry Analysis, Saturation Magnetization Values Obtained at 300 K, g_{efec} of the Solid Product, and g_{efec} Shifting (Δg_{efec}) of the Embedded Paper for the Different Magnetite Nanoparticle Samples

sample	D_{TEM} (nm)	% organic content	M_s (emu/gFe_3O_4) RT	g_{efec} (s)	Δg_{efec} (p)
MNP16	7 ± 1	16.1	67.6	2.47	0.380
MNP18	7.1 ± 0.9	18.4	63.9	2.38	0.195
MNP30	4.3 ± 0.7	30.1	70.4	2.18	0.124
MNP40	5.3 ± 0.8	40.6		2.02	0.019
MNP41	4.0 ± 0.4	40.9	70.5	2.04	0.019

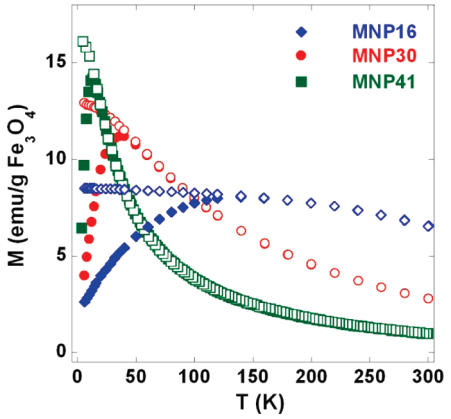

Figure 2. Magnetization as a function of temperature measured in ZFC (solid markers) and FC modes (open markers) of samples MNP16, MNP30, and MNP41 applying a 100 Oe field.

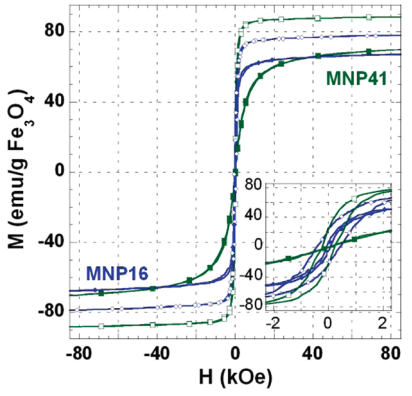

Figure 3. M vs H curves of samples MNP16 and MNP41. Open markers indicate measurements obtained at 5 K and solid markers measurements obtained at 300 K. The inset shows an enlarged view of the low-field region.

In $M(H)$ curves of the samples (Figure 3), the absence of hysteresis observed in the magnetization curves registered at room temperature and the fact that saturation is not achieved at high fields, would be in agreement with a superparamagnetic behavior, as expected for NPs with sizes below the single domain critical value.[24] Nevertheless, and contrary to the expected for superparamagnetic samples, magnetization saturation is easily reached as deduced from the slope of the curves. This phenomenon is more pronounced in MNP16 sample, suggesting stronger interparticle interactions, also deducible from ZFC/FC measurements.

At temperatures well below T_B, the hysteresis appears and, consequently the superparamagnetism disappears, as the thermal energy is no longer sufficient to overcome the magnetic anisotropy energy. The coercive field values observed for MNP16 and MNP41 are 440 and 281 Oe, respectively, higher than expected, most probably due to surface effects.[25] What is more, the higher coercivity value obtained for MNP16 sample is in good accord with the ferromagnetic-like behavior previously remarked and the bigger size of MNP16 nanoparticles.

As the magnetization of an ensemble of non interacting single domain particles in the superparamagnetic regime, each with a certain magnetic moment, can be represented by a Langevin function, experimental data was fitted to a weighted sum of Langevin functions assuming a Gaussian size distribution as confirmed by TEM data.[26] The majority of samples gave acceptable χ^2 values and parameters such as particle average size, its deviation and saturation magnetization values were obtained from the fitting (Supporting Information). The obtained values for the average diameter are close to those estimated from TEM measurements. By contrast, standard deviation values are particularly high, specially, for some of the samples (MNP16), which suggests the existence of magnetic interactions not considered on the applied theoretical model. Additionally, saturation magnetization values are similar to those obtained experimentally and vary depending on the sample, being in most cases close to those reported for bulk magnetite at room temperature (92 emu/g)[27] and similar to the values found for nanoparticles of the same nature.[28]

Aiming to obtain additional and complementary microscopic magnetic information, electron magnetic resonance studies were performed on the samples. The registered room temperature EMR spectra of the solid samples (Figure 4) show an intense and slightly asymmetric line, in agreement with previous studies,[29] that could consist of a superposition of a narrow and a broad component or even a sum of different contributions originated from the small size dispersion in the samples. An additional significant feature appears in some of the spectra consisting of a weak resonance line in the vicinity of 1600 G which origin will be tackled latter. The position of the main resonance field, H_r, and correspondingly the derived effective g value, g_{efec}, (Table 1) as well as the peak to peak line width, ΔH_{pp}, vary depending on the sample. The observed tendency is a broadening of the signal and a shifting from the position at $g_{efec} = 2.0$, corresponding to samples with ideal superparamagnetic behavior, to lower fields with decreasing organic content. The observed trend is in good accord with macroscopic magnetic measurements and is probably a consequence of an increasing interparticle interaction in samples with lower organic content.

It should be highlighted the shape and position dependence of the signal with the amount of sample deposited in the sample holder. Accordingly, the less quantity of sample is used, the best homogeneity of the dispersion is achieved, with no formation of

dx.doi.org/10.1021/cm200253k |*Chem. Mater.* 2011, 23, 2879–2885

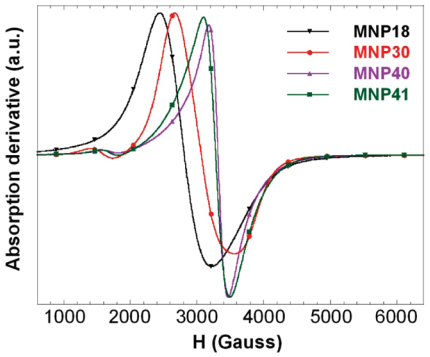

Figure 4. Room-temperature EMR spectra of solid samples.

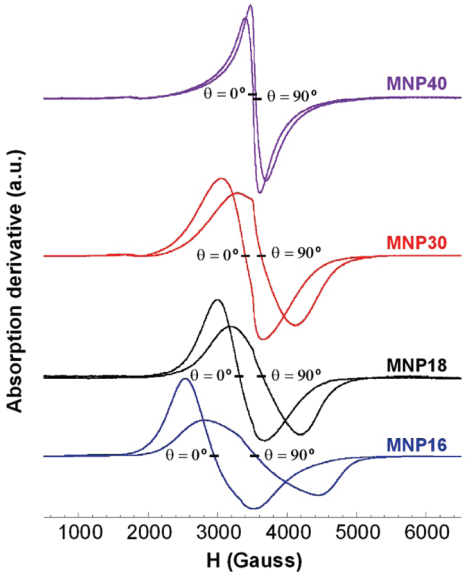

Figure 5. Room-temperature EMR spectra of the nanoparticle suspension embedded paper measured in plane ($\theta = 0°$) and out of plane ($\theta = 90°$) for different samples.

aggregates. Under these conditions, the shape of the signal narrows and displaces toward higher magnetic field values. This fact evidences the importance of the sample handling in an EMR experiment. In order to search for a reproducible measurement method, previous studies involving nanoscale magnetic particles had recourse to the use of a matrix to embed the particles.[30] In our case, we have refined NP disposition either embedding the samples in a piece of paper or depositing them in a polymer film forming a monolayer, as described in the previous section.

Analysis of room temperature EMR spectra of nanoparticles embedded in paper (Figure 5) show a narrowing of the signal compared to previous results. The H_r and ΔH_{pp} values show an angular dependence as follows: when the sample is placed parallel to the applied field ($\theta = 0°$ orientation) a shifting to lower values of g_{efec} is observed, and the application of the magnetic field perpendicular ($\theta = 90°$) to the sample shifts g_{efec} to higher values. The appearance of this angular dependence corroborates the observed ferromagnetism is not solely due to possible aggregates in the sample but reveals that magnetic dipolar interactions play an important role in these samples. To better describe the results, the shifting between 0 and 90° will be referred as Δg_{efec}. We note this value is correspondingly higher

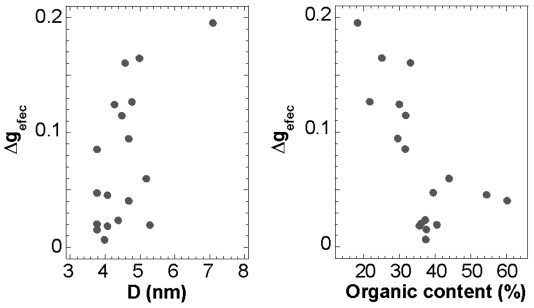

Figure 6. Diameter and organic content dependence of the g_{efec} shifting from out of plane to in plane for a series of synthesized magnetite nanoparticle samples.

in those samples that showed a higher g_{efec} when the solid product is measured (Table 1), and moreover, it gets higher as the organic content decreases, as can be appreciated in Figure 5. To clarify the nature dependence of this parameter, we have measured this value on a series of samples showing different features and when plotting parameter Δg_{efec} separately, as a function of diameter and organic content, we clearly notice that the factor determining the strength of magnetic interactions is the organic content, although it is weakly affected by the diameter in the studied size range (Figure 6). This reinforces the idea of a better isolation among the particles as the organic content increases.

In recent studies, angle-dependent EMR has been performed in iron oxide nanoparticles encapsulated within protein cages after cooling in a 1 T field in order to align the particles.[31] Therein, interparticle interaction as well as demagnetization field was minimized and H_r displacement was used to calculate the anisotropy field and anisotropy density which increases with decreasing particle size. The size of the nanoparticles synthesized in the present work is small enough to also suggest that surface anisotropy plays an important role in the magnetic response of the nanoparticles. Nevertheless, the relation between the shift of the resonance field and the organic matter content suggests that dipolar interactions could be responsible of the observed ferromagnetic resonance. It has been observed that strong magnetic dipole interactions between magnetic nanoparticles, which would be superparamagnetic as isolated, can result in a collective state of nanoparticles.[23]

Another feature to be considered in the spectra of some samples is the appearance of weaker spectral lines at fields corresponding to the half of the resonance field value of the main resonance. Figure 7 displays a sequence of spectra as a function of the angle θ for a representative ferromagnetic sample showing the feature cited above. The analogous angular dependence of both signals enables one to discard the origin of the additional line in an impurity typical for paramagnetic Fe^{3+} ions[32] and, instead, is ascribed to a forbidden transition characterized by $\Delta M_s = \pm 2$, in agreement with similar studies reported in the literature.[33,34] The appearance of these signals at half-field as well as the ratio between the relative intensity of the principal signal and the secondary one could be related to the presence of discrete systems such as very small nanoparticles without extended magnetic interactions. In this way, this quantum feature would be observed in dispersed samples with small size and well isolated one from another, as is the case of nanoparticles represented in Figure 7, which present 5.0 ± 0.5 nm in diameter and an organic content of 30.2%.

For samples deposited forming monolayers, room-temperature EMR spectra show more defined signals that barely depend

dx.doi.org/10.1021/cm200253k |*Chem. Mater.* 2011, 23, 2879–2885

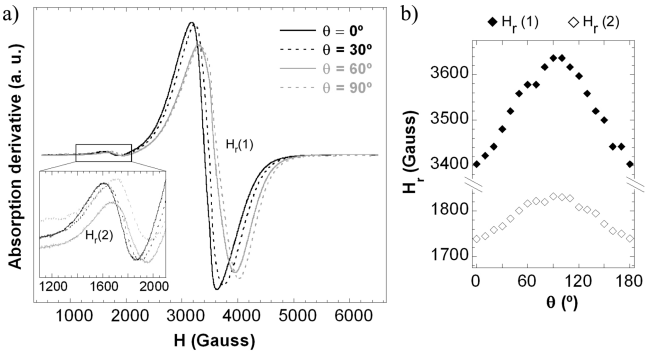

Figure 7. (a) Room-temperature EMR spectra measured at different angles for a representative ferromagnetic sample. The inset illustrates an enlarged view of the angular variation of the smaller signal. (b) Angular evolution of the resonance field values for the main and the smaller lines.

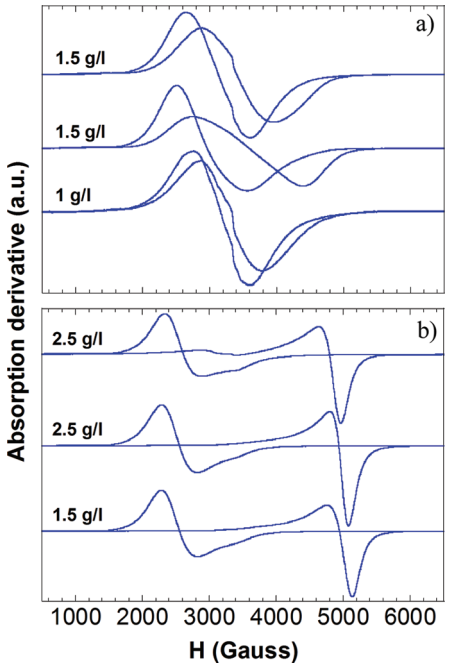

Figure 8. (a) Room-temperature EMR spectra of the sample MNP16 embedded in paper measured in plane ($\theta = 0°$) and out of plane ($\theta = 90°$) for three different preparations using the same nanoparticle concentration for two of them. (b) Room-temperature EMR spectra of the sample MNP16 deposited on a film forming a monolayer measured in plane ($\theta = 0°$) and out of plane ($\theta = 90°$) for three different preparations using the same nanoparticle concentration for two of them.

on the concentration of the solution used for the monolayer preparation (Figure 8). Remarkably, the resonance lines recorded in plane ($\theta = 0°$) and out of plane ($\theta = 90°$) display a major Δg_{efec} compared to the values obtained with previously studied sample handling methods. In this case, the 2D assembly of nanoparticles yields an anisotropic behavior. While in previous dispositions interparticle interactions were randomly oriented, in 2D systems interactions occur mainly in a preferred plane. This finding indicates that individual particles in the monolayer remain tightly held and are not able to freely rotate toward the direction of the magnetization field.

The thermal evolution of the resonance signal has also been measured. For this task, we focused our attention on two samples

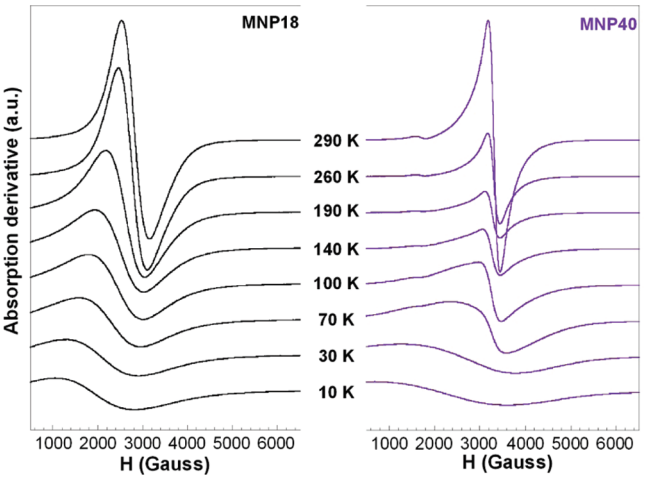

Figure 9. EMR spectra of samples MNP18 and MNP40 at different temperatures.

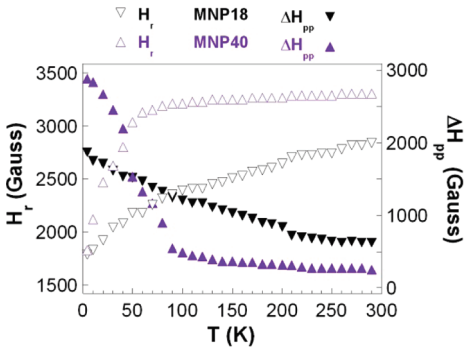

Figure 10. Temperature dependence of resonance field, H_r, and line width, ΔH_{pp}, for samples MNP18 (open and solid inverted triangles) and MNP40 (open and solid triangles).

with g values ascribed to different behaviors. Figure 9 shows the registered spectra for the solid samples MNP18 and MNP40 and essentially both describe a broadening and a shift of the signal to lower magnetic field values when cooling down the samples. However, slight differences can be distinghished in the variation of the resonance field and the line width as a function of temperature (Figure 10). That is, as the temperature diminishes, while sample MNP18 presents a progressive variation in the temperature range studied, sample MNP40 displays a negligible evolution down to 90 K for ΔH_{pp} and 60 K for H_r, and below, a sharp change occurs. This observation agrees well with the thermal evolution expected for ferromagnetic and superparamagnetic systems, respectively. Thermal evolution of the signals has demonstrated that the intensity of the $g = 4$ signal decreases upon lowering the temperature as observed in similar systems,[35] showing an opposite behavior to that expected for a paramagnetic system. In this sense, the EMR has been proved as a powerful technique not only to elucidate ferromagnetic contributions but also to corroborate the quantum nature of these systems.

4. CONCLUSIONS

Herein, we present a systematic study of the influence of the different synthetic parameters on the final particle size and organic content of the magnetite nanoparticles and a full characterization of their magnetic behavior by means of EMR. The optimization of

these measurements has proved as a powerful technique to distinguish magnetic contributions that otherwise were not clear by *dc* magnetization measurements. Accordingly, monodisperse magnetite nanoparticles with average particle size between 3.5 nm up to 7 nm and organic content ranging from 16.1 to 40.9% have been prepared. Magnetization curves revealed features typical of a superparamagnetic behavior, nevertheless, significant discrepancies made necessary to further study the magnetic properties by means of electron magnetic resonance. This technique clearly evidences the organic content dependence of the magnetic character, going from superparamagnetic to ferromagnetic as the organic matter decreases, indicating the importance of interparticle interactions when the nanoparticle surface gets naked. Likewise, it has been found that nanoparticle disposition in the EMR experiment is of key importance to get reproducible results, which has required the development of sample preparation approaches for the experiment. Angular dependent EMR measurements have demonstrated the correlation between the main resonance line and the weak resonance line. This weak line has been ascribed to a $\Delta M_S = \pm 2$ forbidden transition, which would be ascribed to quantum confinement in small systems with no possibility of extended interactions.

■ ASSOCIATED CONTENT

Supporting Information. Saturation magnetization and nanoparticle sizes determined by fitting magnetization data to Langevin function for the different magnetite nanoparticle samples. Preparation scheme of the magnetite monolayer film and TEM micrograph of the resulting monolayer. Thermogravimetric measurements for MNP18, MNP30, MNP40, MNP41, and MNP16 samples. This material is available free of charge via the Internet at http://pubs.acs.org.

■ AUTHOR INFORMATION

Corresponding Author

*Tel.: 00 3494 6012703. E-mail: teo.rojo@ehu.es.

■ ACKNOWLEDGMENT

This work was supported by institutional funding from the Ministerio de Educación y Ciencia and Basque Government under Projects MAT2007-66737-C02-01, MAT2010-19942 and GIC-IT-382-07. J. Salado thanks MEC for a predoctoral fellowship.

■ REFERENCES

(1) Schmid, G. *Nanoparticles: From Theory to Application*; Wiley-VCH: Weinheim, Germany, 2004.
(2) Roduner, E. *Chem. Soc. Rev.* **2006**, *35*, 583–592.
(3) Rao, C. N. R.; Kulkarni, G. U.; Thomas, P. J.; Edwards, P. P. *Chem.—Eur. J.* **2002**, *8*, 28–35.
(4) Demortière, A.; Panissod, P.; Pichon, B. P.; Pourroy, G.; Guillon, D.; Donnio, B.; Bégin-Colin, S. *Nanoscale* **2011**, *3*, 225–232.
(5) Mornet, S.; Vasseur, S.; Grasset, F.; Duguet, E. *J. Mater. Chem.* **2004**, *14*, 2161–2175.
(6) Dobson, J. *Drug. Dev. Res.* **2006**, *67*, 55–60.
(7) Derfus, A.; von Maltzahn, G.; Harris, T.; Duza, T.; Vecchio, K.; Ruoslahti, E.; Bhatia, S. *Adv. Mater.* **2007**, *19*, 3932–3936.
(8) Jordan, A.; Scholz, R.; Maier-Hauf, K.; Johannsen, M.; Wust, P.; Nadobny, J.; Schirra, H.; Schmidt, H.; Deger, S.; Loening, S.; Lanksch, W.; Felix, R. *J. Magn. Magn. Mater.* **2001**, *225*, 118–126.
(9) Huh, Y.-M.; Jun, Y.-W.; Song, H.-T.; Kim, S.; Choi, J.-S.; Lee, J.-H.; Yoon, S.; Kim, K.-S.; Shin, J.-S.; Suh, J.-S.; Cheon, J . *J. Am. Chem. Soc.* **2005**, *127* (35), 12387–12391.
(10) Laurent, S.; Forge, D.; Port, M.; Roch, A.; Robic, C.; Vander Elst, L.; Muller, R. N. *Chem. Rev.* **2008**, *108*, 2064–2110.
(11) Park, J.; An, K.; Hwang, Y.; Park, J.-G.; Noh, H.-J.; Kim, J.-Y.; Park, J.-H.; Hwang, N.-M.; Hyeon, T. *Nat. Mater.* **2004**, *3*, 891–895.
(12) Sun, S.; Zeng, H. *J. Am. Chem. Soc.* **2002**, *124* (28), 8204–8205.
(13) Sun, S.; Zeng, H.; Robinson, D. B.; Raoux, S.; Rice, P. M.; Wang, S. X.; Li, G. *J. Am. Chem. Soc.* **2004**, *126* (1), 273–279.
(14) Bean, C. P.; Livingston, J. D. *J. Appl. Phys.* **1959**, *30* (4), 120S–129S.
(15) Néel, L. *C. R. Acad. Sci. Paris* **1949**, *228*, 64–66.
(16) Batlle, X.; Labarta, A. *J. Phys. D: Appl. Phys.* **2002**, *35*, R15–R42.
(17) Garitaonandia, J. S.; Insausti, M.; Goikolea, E.; Suzuki, M.; Cashion, J. D.; Kawamura, N.; Ohsawa, H.; Gil de Muro, I.; Suzuki, K.; Plazaola, F.; Rojo, T. *Nano Lett.* **2008**, *8* (2), 661–667.
(18) Nakata, K.; Hu, Y.; Uzun, O.; Bakr, O.; Stellacci, F. *Adv. Mater.* **2008**, *20*, 4294–4299.
(19) Fittipaldi, M.; Sorace, L.; Barra, A.-L.; Sangregorio, C.; Sessoli, R.; Gatteschi, D. *Phys. Chem. Chem. Phys.* **2009**, *11*, 6555–6568.
(20) Glaria, A.; Kahn, M. L.; Lecante, P.; Barbara, B.; Chaudret, B. *ChemPhysChem* **2008**, *9*, 776–780.
(21) Puntes, V. F.; Krishnan, K. M.; Alivisatos, P. *Appl. Phys. Lett.* **2001**, *78*, 2187–2189.
(22) Park, J.; An, K.; Hwang, Y.; Park, J. G.; Noh, H. J.; Kim, J. Y.; Park, J. H.; Hwang, N. M.; Hyeon, T. *Nat. Mater.* **2004**, *3*, 891–895.
(23) Morup, S.; Hansen, M. F.; Frandsen, C. *Beilstein J. Nanotechnol.* **2010**, *1*, 182–190.
(24) Ge, J.; Hu, Y.; Biasini, M.; Beyermann, W. P.; Yin, Y. *Angew. Chem., Int. Ed.* **2007**, *46*, 4342–4345.
(25) Guardia, P.; Batlle-Brugal, B.; Roca, A. G.; Iglesias, O.; Morales, M. P.; Serna, C. J.; Labarta, A.; Batlle, X. *J. Magn. Magn. Mater.* **2007**, *316*, e756–e759.
(26) Ferrari, E. F.; da Silva, F. C. S.; Knobel, M. *Phys. Rev. B* **1997**, *56*, 6086–6093.
(27) Cullity, B. D. *Introduction to Magnetic Materials*; Addison-Wesley: Boston, 1972.
(28) Roca, A. G.; Marco, J. F.; Morales, M. P.; Serna, C. J. *J. Phys. Chem. C* **2007**, *111*, 18577–18584.
(29) Salado, J.; Insausti, M.; Gil de Muro, I.; Lezama, L.; Rojo, T. *J. Non-Cryst. Solids* **2008**, *354*, 5207–5209.
(30) Koksharov, Y. A.; Gubin, S. P.; Kosobudsky, I. D.; Yurkov, G. Y.; Pankratov, D. A.; Ponomarenko, L. A.; Mikheev, M. G.; Beltran, M.; Khodorkovsky, Y.; Tishin, A. M. *Phys. Rev. B* **2000**, *63*, 012407.
(31) Li, H.; Klem, M. T.; Sebby, K. B.; Singel, D. J.; Young, M.; Douglas, T.; Idzerda, Y. U. *J. Magn. Magn. Mater.* **2009**, *321*, 175–180.
(32) Berger, B.; Kliava, J.; Bissey, J. C.; Baietto, V. *J. Appl. Phys.* **2000**, *87*, 7389–7396.
(33) Noginova, N.; Barnakov, Y.; Radocea, A.; Atsarkin, V. A. *ArXiv. org, e-Print Archive, Condensed Matter*, **2009**, 1−18, arXiv:0911.1752v1 [cond-mat.mes-hall].
(34) Noginova, N.; Weaver, T.; Giannelis, E. P.; Bourlinos, A. B.; Atsarkin, V. A.; Demidov, V. V. *Phys. Rev. B* **2008**, *77*, 014403.
(35) Ceci, P.; Chiancone, E.; Kasyutich, O.; Bellapadrona, G.; Castelli, L.; Fittipaldi, M.; Gatteschi, D.; Innocenti, C.; Sangregorio, C. *Chem.—Eur. J.* **2010**, *16*, 709–717.